Differential Dynamic Modulus of Polyisobutylene with High Molecular Weight. 3. Stress Development after the Onset of Steady Shear Flow

Yoshinobu Isono,* Hirotaka Kawaura, Toshio Komiyatani, and Teruo Fujimoto

Department of Materials Science and Technology, Nagaoka University of Technology, Nagaoka, Niigata 940-21, Japan

Received September 17, 1990; Revised Manuscript Received March 11, 1991

ABSTRACT: Shear stress development after the onset of steady shear flow was measured at 20 °C for a polyisobutylene with viscosity-average molecular weight 9.6×10^5 at shear rates from 3.5×10^{-4} to 3.5×10^{-3} s^{-1}. The initial parts of the stress growth coefficient curves at different shear rates composed a single curve. Simultaneous measurements of the differential dynamic moduli, $G'(\omega,\dot{\gamma};t)$ and $G''(\omega,\dot{\gamma};t)$, were made during the stress development process by intermittently superposed small sinusoidal oscillations at 0.1 Hz, which falls in the middle of the plateau zone. At a relatively low shear rate, both G' and G'' showed constant values just the same as in linear viscoelasticity until a certain time elapsed. This time region corresponded to that in the above single curve. Then G' began to decrease and G'' to increase. Corresponding to these changes in G' and G'', the stress growth coefficient began to deviate from the single curve. The critical shear strain was near 0.15 and approximately independent of shear rate. It was concluded that the original entanglement structure of the linear polymer remains unchanged until a certain critical strain is accumulated and the nonlinear behavior in stress development corresponds to a change in the entanglement structure.

Introduction

In previous works, it was found that the entanglement structure changes with the strain given to the material by measurements of the differential dynamic modulus during the stress relaxation process in shearing deformations.[1-3] In small shearing deformations, it was confirmed that the density of the entanglements remains constant.[1,2]

In steady shear flow, too, the effective entanglement density is expected to be independent of shear rate, if the shear rate is low enough. If the shear rate is high, i.e., in the nonlinear region, the entanglement density may vary with shear rate but remains constant in the steady state.[4-13]

In the stress development phenomena after onset of steady shear flow, it may be speculated that the structure is changed not only with shear rate but also with time. The initial entanglement structure of the material may be transformed into a different structure during a transient process, and the transition from the initial state to the final state would occur if the strain in the material reaches a critical value, as pointed out by Nagasawa et al.[7-11] Such an idea has been experimentally supported by observing the stress development or stress relaxation after a stepwise change of shear rate from a value of $\dot{\gamma}_1$ (including $\dot{\gamma}_1 = 0$) to another value of $\dot{\gamma}_2$[7-15] and also by analysis of creep and creep recovery.[16] On the basis of this model, moreover, Nagasawa et al. pointed out that the memory function or after-effect function should be defined for the entanglement structure of the material.[7-11,14,15]

The purpose of this work is to test the idea of such a "network-rupture model" by measuring the differential dynamic modulus during stress development processes after the onset of steady shear flow. The change in the entanglement structure of polymeric materials may be observed in the stress development processes more easily than in stress relaxation processes.

Materials and Method

A sample, polyisobutylene L-80 (Exxon Chemicals Company), and the apparatus used, a Weissenberg Rheogoniometer R-18 (Sangamo Controls Ltd.), were the same as in the preceding two works in this issue.[2,3]

In this work, a Couette type of shear deformation was adopted. Figure 1 shows a sketch of the cross section of the specially designed device for this type of deformation. The hatched portion is the ring-shaped sample. The inner and outer radii were 4 and 14 mm, respectively. The cross-hatched portion is the deformed part of the sample. The inner and outer radii of this deformed part were 9.25 and 11 mm, respectively. The sample thickness was typically 1 mm. The inner and outer parts of the sample ring were separately sandwiched and fixed with a cyanoacrylate glue. The inner bob and the outer cup can move independently. So shear deformation can be easily obtained by their relative rotation around the axis or relative displacement along the axis. In this work, a relative rotation was adopted. The sample was molded at about 100 °C in sheets. Ring-shaped samples were cut by a double punch.

A sketch of the experimental procedure is shown in Figure 2. Before shearing, the dynamic moduli, $G'(\omega,0)$ and $G''(\omega,0)$, where 0 denotes the zero static strain, were measured. A shear flow with a shear rate, $\dot{\gamma}_0$, was started at time zero. At intervals, small sinusoidal deformations with a shear amplitude of γ_1 at a radian frequency, ω, were superimposed. Total strain, $\gamma(t)$, and total stress, $\sigma(t)$, are given as

$$\gamma(t) = \dot{\gamma}_0 t + \gamma_1 \sin(\omega t) \tag{1}$$

$$\sigma(t) = \sigma(\dot{\gamma}_0;t) + \sigma_1 \sin(\omega t + \delta) \tag{2}$$

The stress growth coefficient and differential dynamic modulus are defined by

$$\eta(\dot{\gamma}_0;t) = \sigma(\dot{\gamma}_0;t)/\dot{\gamma}_0 \tag{3}$$

$$G'(\omega,\dot{\gamma}_0;t) = (\sigma_1/\gamma_1)\cos\delta \tag{4}$$

$$G''(\omega,\dot{\gamma}_0;t) = (\sigma_1/\gamma_1)\sin\delta \tag{5}$$

At time t_1, when the magnitude of shear reached 2, the flow was stopped. After t_1, stress relaxation was observed. If $\dot{\gamma}_0$ is very high, this experiment corresponds to a step strain experiment at $\gamma = 2$.

Experiments were made at various values of $\dot{\gamma}$ varying from 3.5×10^{-4} to 3.5×10^{-3} s^{-1}, which were estimated at the mean radius of the deformed part of the sample. The details for estimation of shear rate will be explained in the next section. The strain amplitude of the superposed oscillation was less than

0024-9297/91/2224-4437$02.50/0

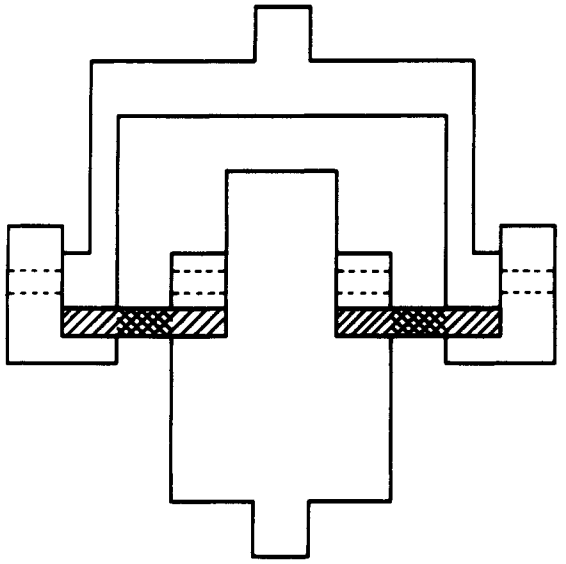

Figure 1. Rough sketch of the device for a Couette type of shear deformation, designed and made by ourselves. Broken lines show the positions of setscrews. The hatched and cross-hatched portions are a ring-shaped sample and a deformed part of the sample, respectively.

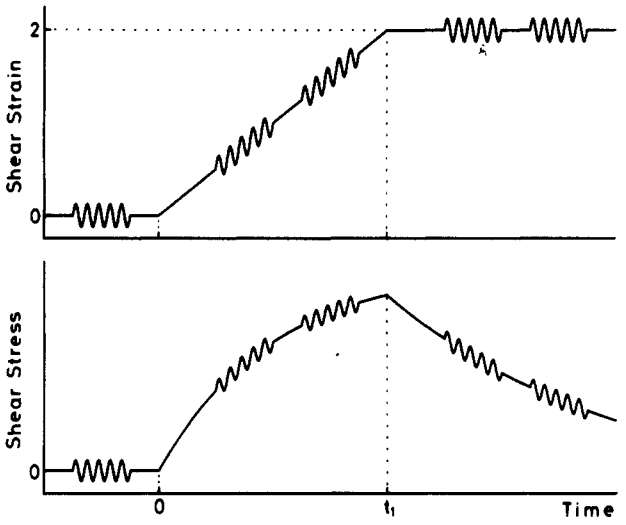

Figure 2. Schematic diagram of the stress development and stress relaxation with superposed small oscillations.

0.03. In this range of oscillatory amplitude, the differential dynamic modulus was found to be independent of the amplitude, even if the shear rate was high. The frequency was 0.1 Hz, which corresponds to a time scale in the plateau zone.[2] Measurements were made at 20 °C.

Results and Discussion

Figure 3 shows the results after cessation of steady shear flow at $\gamma = 2$. The relaxation modulus $G(\gamma,\dot{\gamma};t-t_1)$ depends on the shear rate as shown in the top panel. It lowers as $\dot{\gamma}$ decreases. These curves converge at the long-time region and agree with the values of the step strain experiment at $\gamma = 2$ shown by the broken line. The corresponding behaviors were observed on $G'(\omega,\gamma,\dot{\gamma};t-t_1)$ and $G''(\omega,\gamma,\dot{\gamma};t-t_1)$, too, as shown in the bottom two panels.

Figure 4 shows the coefficient $S/(b\dot{\alpha})$, where S is the torque, b is the form factor, and $\dot{\alpha}$ is the angular velocity (rad·s^{-1}), respectively. In the linear viscoelasticity, this corresponds to the stress growth coefficient. There are, however, distributions of strain and stress in a radial direction in the present experiments. The distributions can be estimated with the single-bob method by Krieger and Maron.[17-19]

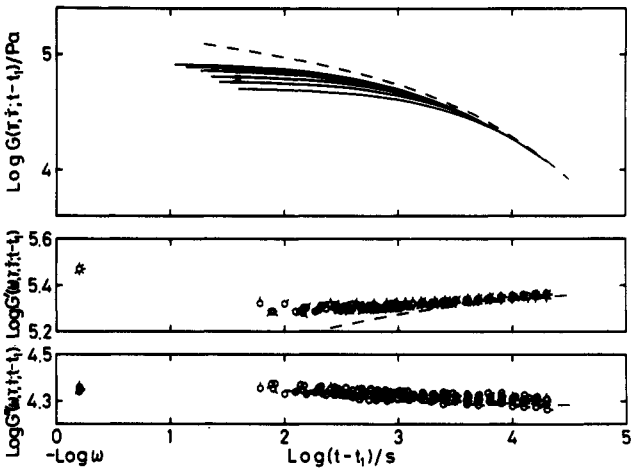

Figure 3. Double-logarithmic plots of $G(\gamma,\dot{\gamma};t-t_1)$, $G'(\omega,\gamma,\dot{\gamma};t-t_1)$, and $G''(\omega,\gamma,\dot{\gamma};t-t_1)$ against $t-t_1$ for six different shear rates. In the top panel, shear rates are 3.5×10^{-3} s^{-1} for the first solid line at the top, then 2.2×10^{-3}, 1.4×10^{-3}, 8.8×10^{-4}, 5.5×10^{-4}, and 3.5×10^{-4} s^{-1} for the remaining five lines, respectively, from top to bottom. In the bottom panels, pip up, $\dot{\gamma} = 3.5 \times 10^{-4}$ s^{-1}; successive 45° rotations clockwise, 5.5×10^{-4}, 8.8×10^{-4}, 1.4×10^{-3}, 2.2×10^{-3}, and 3.5×10^{-3} s^{-1}. These values of the shear rate are the ones at the mean radius, estimated in Figure 5, and the related analysis (see text). $G'(\omega,0)$ and $G''(\omega,0)$ denote measurements before shearing, at the frequency shown on the abscissa at the left ($\log \omega = -0.2$, $\nu = 0.1$ Hz). Broken lines show the curves of $G(\gamma,t)$, $G'(\omega,\gamma;t)$, and $G''(\omega,\gamma;t)$ for the sample L-80 in the step strain experiment at $\gamma = 2$.[3]

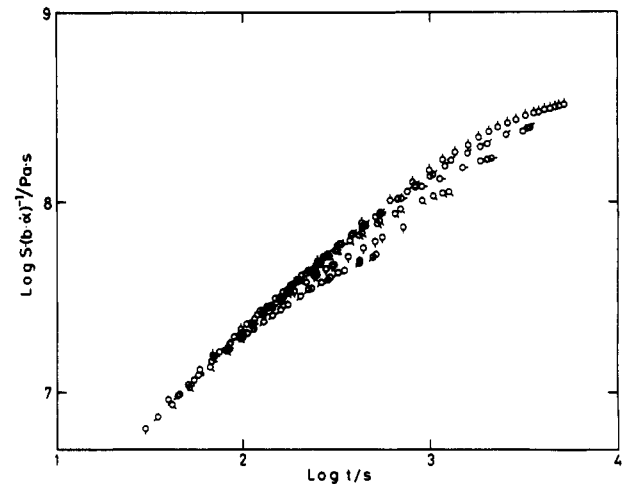

Figure 4. Double-logarithmic plots of the coefficient $S/(b\dot{\alpha})$ against t for six different speeds of rotation of the inner bob. Pip up, speed of rotation is 5.96×10^{-4} rpm; successive 45° rotations clockwise, 9.43×10^{-4}, 1.50×10^{-3}, 2.37×10^{-3}, 3.75×10^{-3}, and 5.96×10^{-3} rpm.

Figure 5 shows three examples of the time variation of shear rate distribution for different speeds of rotation. The rate of shear has a maximum and a minimum at the inner and outer radii, respectively. These extremes are shown by solid lines. The difference between the maximum and the minimum values remains constant in the beginning but becomes wider as time elapses. However, the shear rate at the mean radius shown by the broken line remains constant. The extremes differ from the value at the mean radius by approximately ±18 or ±40%. The stress also has distribution in the radial direction. It has a maximum and a minimum at the innner and outer radii, respectively, depending on the inverse square of the radial distance from the center, so the distribution in the stress growth coefficient is expected to be not so broad.

Figure 6 shows three examples of the distribution in the

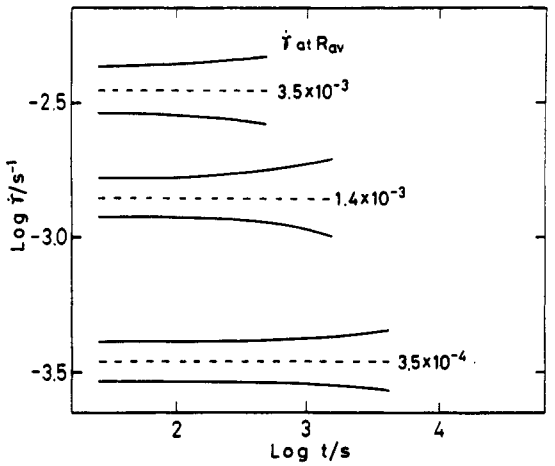

Figure 5. Double-logarithmic plots of the shear rate distribution in a radial direction against t for three different speeds of rotation of the inner bob, 5.96×10^{-3}, 2.37×10^{-3}, and 5.96×10^{-4} rpm, from top to bottom. In each combination of curves, the upper and lower solid lines show the shear rate at the inner and outer radii, respectively. Broken lines show the shear rates at the mean radius.

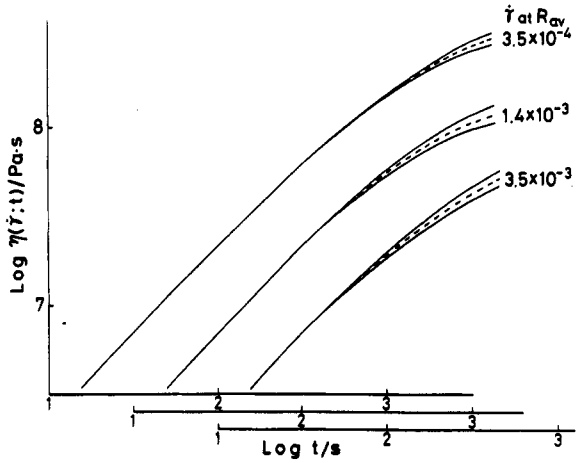

Figure 6. Double-logarithmic plots of the stress growth coefficient development distribution in a radial direction against t for three different speeds of rotation. Curves are shifted along the abscissa to avoid overlapping. In each combination of curves, the upper and lower solid lines show the coefficient at the outer and inner radii, respectively. Broken lines show the coefficient at the mean radius.

stress growth coefficient for three different speeds of rotation. In this figure, the curves are shifted along the abscissa to avoid overlapping. In each combination of curves, the upper and lower solid lines show the values at the outer and inner radii, respectively. The broken line shows the value at the mean radius. We can find that the extremes in the coefficient differ from the mean value at most by ±8 or ±13% in the present measurements. It is noted that there is no distribution in stress growth coefficient in the radial direction at the beginning.

The stress growth coefficients after onset of steady shear flow estimated at the mean radius are plotted double-logarithmically against time for various shear rates in the top panel of Figure 7. The curves form a single curve irrespective of the shear rate at the initial state of rotation or in the region of $t \to 0$. This agrees with the results of Kajiura et al.,[7,9] Isono and Nagasawa,[11] Menezes and Graessley,[12,13] and Takahashi et al.[14,15] From the results of Figures 6 and 7, it is clear that the initial part of the stress growth coefficient curve is in the linear region, although the whole growth curve in the linear region was not obtained in the present experiment. After a certain

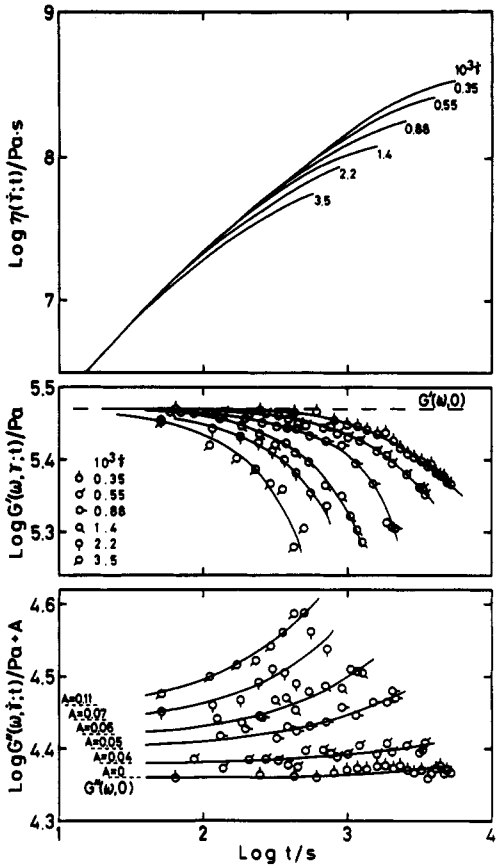

Figure 7. Double-logarithmic plots of $\eta(\dot{\gamma},t)$, $G'(\omega,\dot{\gamma};t)$, and $G''(\omega,\gamma;t)$ against t for six different shear rates. The shear rates estimated at the mean radius are denoted in the figure. Broken lines in the middle and the bottom panels denote the values of $G'(\omega,0)$ and $G''(\omega,0)$, respectively. In the bottom panel, plots are shifted along the ordinate by a factor of A denoted in the panel.

time elapses, the coefficient begins to deviate from the single curve. The deviating time depends on the shear rate. As the shear rate increases, the deviating time becomes shorter.

In the second and the third panels of Figure 7, the differential dynamic moduli, $G'(\omega,\dot{\gamma};t)$ and $G''(\omega,\dot{\gamma};t)$, measured during the stress growth experiments are plotted double-logarithmically against time for various shear rates. For the lowest shear rate, the stress growth coefficient develops in a linear manner until about 400 s ($\log t = 2.6$). Until this time, $G'(\omega,\dot{\gamma};t)$ shows a constant value that is in agreement with the value obtained at the equilibrium state. As time proceeds, it begins to deviate from the constant value. In $G''(\omega,\dot{\gamma};t)$, too, similar behavior can be found, although data are somewhat scattered and the deviation from $G''(\omega,0)$ is fairly small. For the other shear rates, we can find the same features.

In Figure 8, the values of $G'(\omega,\dot{\gamma};t)$ and $G''(\omega,\dot{\gamma};t)$ are plotted double-logarithmically against γt, that is, the shear strain. The initial values of $G''(\omega,0)$ as well as $G'(\omega,0)$ should have been the same for each sample. In practice, $G'(\omega,0)$ showed almost the same value for each sample. But $G''(\omega,0)$ varied by about 5%. For comparison, however, all those values of G'' were arbitrarily adjusted to make $G''(\omega,0)$ match the average ($\log G''(\omega,0) = 4.35$ Pa) in Figure 8. At small magnitudes of shear, both G' and G'' take the original linear values, $G'(\omega,0)$ and $G''(\omega,0)$, respectively. When the shear strain reaches a certain critical value, nonlinear behavior appears. Thus, it may be concluded that the original entanglement structure of linear polymer remains unchanged until a certain critical strain is accumulated.

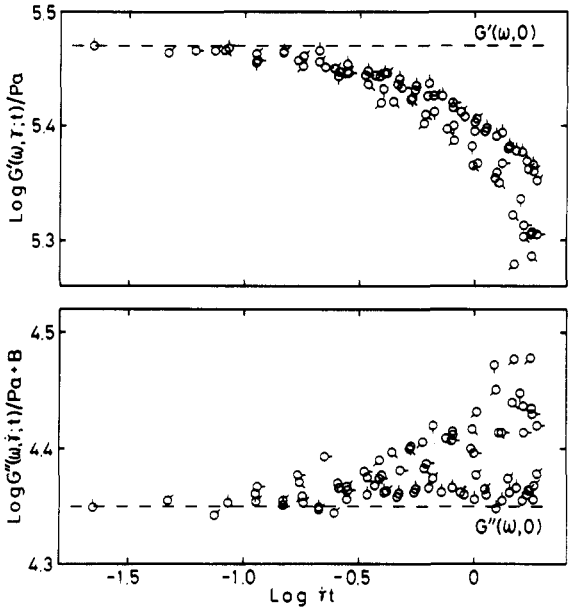

Figure 8. Double-logarithmic plots of $G'(\omega,\dot{\gamma};t)$ and $G''(\omega,\dot{\gamma};t)$ against $\dot{\gamma}t$. Symbols are the same as in Figure 7. In the lower panel, plots are shifted along the ordinate by a factor of B. Pip up, $B = -0.01$; successive 45° rotations clockwise, 0.01, 0, −0.01, −0.02, and 0.01 (see text).

At large shear strains, curves are not superposed. It is clear that the structure of the polymeric materials is not only determined by the magnitude of strain but also affected by the strain history of the material. It may be also concluded that the nonlinear behavior in stress development corresponds to a change in entanglement structure.

Finally, it may be remarked that the critical shear strain where nonlinear behavior begins to appear is around 0.15 and independent of shear rate. This value is very close to the value where the experimentally observed relaxation modulus beings to depend on strain.[2] Such an existence of a critical strain for deviations from the linear behavior has been reported by Berry et al. in creep experiments[16] and Kajiura et al.,[7,9] Isono and Nagasawa,[11] Menezes and Graessley,[12,13] and Takahashi et al.[14,15] in the onset of steady shear flow experiments, and a discussion on onset of nonlinear flow behavior has been given by Ferry.[20] However, the reported critical values are much larger than that in the present work. The magnitude of the critical shear strain may be determined carefully. At least, however, it is lower than unity.

Acknowledgment. We are greatly indebted to Professor John D. Ferry of the University of Wisconsin and Professor Mitsuru Nagasawa of the Toyota Institute of Technology for their valuable comments.

References and Notes

(1) Isono, Y.; Ferry, J. D. *J. Rheol.* **1985**, *29*, 273.
(2) Isono, Y.; Itoh, K.; Komiyatani, T.; Fujimoto, T *Macromolecules*, part 1 of a series of 3 in this issue.
(3) Isono, Y.; Shizuru, K.; Fujimoto, T. *Macromolecules*, part 2 of a series of 3 in this issue.
(4) Graessley, W. W. *J. Chem. Phys.* **1967**, *47*, 1942.
(5) Sakai, M.; Fujimoto, T.; Nagasawa, M. *Macromolecules* **1972**, *5*, 786.
(6) Graessley, W. W. *Adv. Polym. Sci.* **1974**, *16*, 1.
(7) Kajiura, H.; Sakai, M.; Nagasawa, M. *J. Soc. Rheol., Jpn.* **1974**, *2*, 123.
(8) Sakai, M.; Kajiura, H.; Nagasawa, M. *Trans. Soc. Rheol.* **1974**, *18*, 323.
(9) Kajiura, H.; Sakai, M.; Nagasawa, M. *Trans. Soc. Rheol.* **1976**, *20*, 575.
(10) Isono, Y.; Kajiura, H.; Nagasawa, M. *J. Rheol.* **1979**, *23*, 79.
(11) Isono, Y.; Nagasawa, M. *Macromolecules* **1980**, *13*, 862.
(12) Menezes, E. V.; Graessley, W. W. *Rheol. Acta* **1980**, *19*, 38.
(13) Menezes, E. V.; Graessley, W. W. *J. Polym. Sci., Polym. Phys. Ed.* **1982**, *20*, 1817.
(14) Takahashi, Y.; Isono, Y.; Noda, I.; Nagasawa, M. *Macromolecules* **1986**, *19*, 1217.
(15) Takahashi, Y.; Isono, Y.; Noda, I.; Nagasawa, M. *Macromolecules* **1987**, *20*, 153.
(16) Berry, G. C.; Hager, B. L.; Wong, C. P. *Macromolecules* **1977**, *10*, 361.
(17) Krieger, I. M.; Maron, S. H. *J. Appl. Phys.* **1952**, *23*, 147.
(18) Krieger, I. M.; Elrod, H. *J. Appl. Phys.* **1953**, *24*, 134.
(19) Krieger, I. M.; Maron, S. H. *J. Appl. Phys.* **1954**, *25*, 72.
(20) Ferry, J. D. *Viscoelastic Properties of Polymers*, 3rd ed.; Wiley: New York, 1980; p 519.